CETRA 2014 28–30 April 2014, Split, Croatia
3rd International Conference on Road and Rail Infrastructure

Influences of characteristic size of contact bodies on rolling contact

Zhiwei Qian, Xiangyun Deng, Zili Li & Rolf Dollevoet
Railway Engineering, Delft University of Technology, the Netherlands

Abstract

The rolling contact of elastic bodies (upper body and lower body) can be analyzed with the Hertz theory and the Kalker's model. It is generally believed that the width of the contact area should be much smaller than the characteristic size of each elastic body, to ensure that the half-space assumption is valid. However the definition of "much smaller" is not that clear. In practice the 3x rule is usually employed, which requires the characteristic size of each elastic body must be at least three times larger than the width of the contact area. This empirical rule is examined in this paper, by looking at the results of the Kalker's model and of a three-dimensional finite element model to study the influences of lower body width on the rolling contact. It is found that the contact behavior predicted by the Kalker's model are still acceptable even when the characteristic size of contact bodies is close to the width of the contact area. This finding extends the applicability of classical quasi-static methods to a wider scope, and thus may simplify the calculation procedures for rolling contact problems.

Keywords: rolling contact, size effects, elastic contact bodies, 3D explicit FEA, wheel-rail interaction

1 Introduction

Frictional rolling contact can be found between wheels and rails, as well as in not well-lubricated bearings and gears. Accurate evaluation of the stress, strain and partial slip due to the contact is important for analyzing wear damage and rolling contact fatigue, and for designing such components [1-3]. The Hertz theory [4] was proposed in 1882 to explain what happens when two elastic bodies touch each other. The elastic deformation of the contact bodies creates an elliptic contact area. The size of the contact ellipse is determined by the normal force on the contact area, the elastic modulus and the principal curvatures of the bodies. In 1926 Carter developed an analytical method to solve the frictional rolling contact problem in two dimensions [5]. In the last decades Kalker established a three-dimensional numerical model based on the Boundary Element Method (BEM), which takes into account arbitrary creepage in the longitudinal and lateral directions, as well as spin [6]. All these theories require that the width of the

contact area should be much smaller than the characteristic size of the contact bodies, in the hope that under such a condition the half-space assumption could be satisfied. However such a condition cannot always be met in practice. For instance, in railway engineering, the curvature of rail gauge r_g and the width of the contact area can be very close, as shown in Figure 1. The width of switch blades can also be close to the width of the contact patch [8]. An interesting question arises: Are those classical theories still applicable to these situations? This paper attempts to answer the question and delivers some findings.

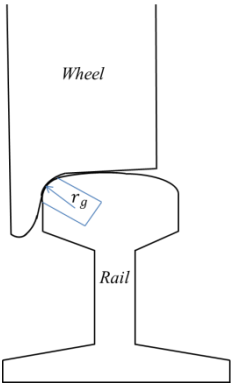

Figure 1. Wheel-rail rolling contact in railways

In recent years Finite Element Analysis (FEA) becomes popular in dealing with rolling contact problems. An advantage of FEA is that the half-space assumption can be dropped. Yan and Fischer [7] compared solution of FEA on normal force with that of the Hertz theory for the case of a standard rail, a crane rail and a switch. They find that the two solutions are well in agreement when either the contact zone does occur in changed surface curvature or the plastic deformation is not taken into account. Wiest [8] computed the normal force distribution for the contact between wheel and rail crossing panel using FEA. He finds that the solutions of FEA, the Hertz theory and the Kalker's model are well agreed, although the size of crossing near contact point is close to the size of contact patch. Zhao and Li [9] created a 3D explicit Finite Element (FE) model solving the rolling contact problem between a wheel and a standard rail. The accuracy of the model is verified and confirmed by comparing with the Kalker's model. Hence the study in this paper makes use of the 3D explicit FE model, taking into account possible influences of lower body width on the rolling contact.

2 3D Finite Element model

2.1 Model description

Two bodies in rolling contact are modeled as shown in Figure 2. The upper body is represented by a cylinder, the radius r_A is 460 mm and the width w_A is 135 mm. The lower body is modeled as a partial cylinder, the radius of the curvature r_B is

150 mm, the height h and the width w are determined according to the rules in the Section 2.2. The upper body is initially placed at the location P, and then starts rolling towards the interest zone MN. The distance between P and M l_{PM} is 160 mm, which is long enough to relax the vibration excited by any initial impact due to imperfect equilibrium of the system to an acceptable level. The length of the interest zone MN l_{MN} is 40 mm. The location O is within the interest zone. The solution of FEA is extracted when the center of upper body arrives at point O. A Cartesian coordinate system $Oxyz$ is created. The rolling direction is aligned with x axis, the vertical direction is indicated by z, and the y direction is determined according to the right-handed rule.

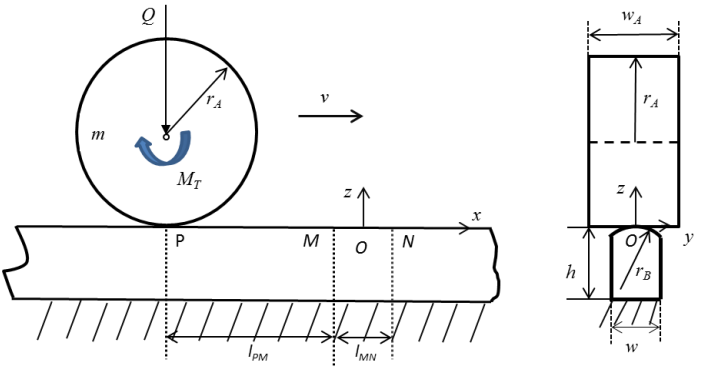

Figure 2. Schematic diagram of the FE model

In the FE model the contact bodies are meshed with 8-node solid elements. Fine mesh of 0.2 mm is assigned to the interest zone of the lower body and part of the upper body to ensure the precision of the solution, as shown in Figure 3. The center of the upper body is constrained in y direction, which means it cannot move laterally. The bottom of the lower body is fixed, and its two ends are restrained in x and y directions.

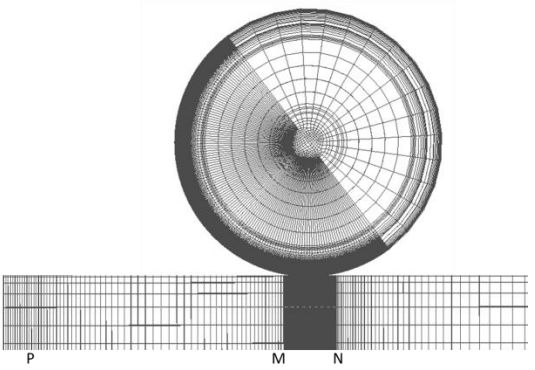

Figure 3. Mesh of the contact system

In this study elastic material properties are assigned to the contact bodies. The Young's modulus is 210 GPa, and the Poisson's ratio is 0.3. The friction coefficient between the contact bodies is 0.5. The mass of the upper body m is 436 kg. The external vertical load on the upper body Q is 78.4 kN. Thus the total static vertical load is 83 kN.

An initial velocity is given to let the upper body start moving from location P. Two scenarios (denoted by scenario A and B) are distinguished, based on whether the driving torque M_T is imposed or not. In the case of scenario A, no tractive force is generated at the contact interface, due to the absence of driving torque. While in scenario B, the driving torque is imposed in such a way that the resulting global tractive force is equal to 25 kN, which is 0.3 times of the total static vertical load.

2.2 Determination of the lower body height and width

The Hertz theory is applied to compute the nominal size of the contact area in the lateral direction, denoted by b_0. The height of the lower body h is fixed at $\frac{h}{2b_0} = 8$. This setting would greatly reduce the boundary effects from the fixed bottom of the lower body. The width of the lower body w is varied at $\frac{w}{2b_0} = 1.1, 2, 8$. These three cases are studied for each scenario, to see how the normal contact pressure, the surface shear stress and the slip-adhesion zone are influenced by the width of the lower body.

2.3 Normalization technique

The normal contact forces in the three cases (with varying $\frac{w}{2b_0}$) shall be the same if the system is considered static, as is the case with Cater [5] and Kalker [6]. In reality, however, the motion of the body will inevitably excite vibrations and waves in the elastic medium, causing fluctuation of the contact force, as shown in Figure 4. The fluctuations will be somehow different for the three cases, though the differences can be minor compared to the total force, if the system is properly damped and is relaxed for a sufficient period of time. Hence normalization technique is applied to cope with such differences and make the three cases comparable.

To elaborate the normalization technique, the case $\frac{w}{2b_0} = 8$ in scenario A is taken as an example. The static vertical load on the upper body is 83 kN. The fluctuating normal contact force is shown in Figure 4. Although a point can be randomly picked up from the curve, as long as it is located within the interest zone, the point O_1 of 88 kN is chosen as an example, which is at the peak of a wave. The FE analysis under this normal force gives the maximum contact pressure of 1524 MPa, denoted by p_{max}. The normal force of 88 kN is also used in the Kalker's model, producing the maximum pressure of 1538 MPa, denoted by p_∞. An index is defined as $\frac{p_{max}}{p_\infty}$, which represents the maximum normalized contact pressure. It is 0.99 in this example.

An assumption is made hereby for the normalization technique, that is within a limited error the normalized value may be considered to be independent of the

point picked up from the curve in the interest zone, provided that the upper and lower bounds of the curve do not differ too much. In other words, it does not matter which point is used for further analysis, as the normalized value almost remains the same.

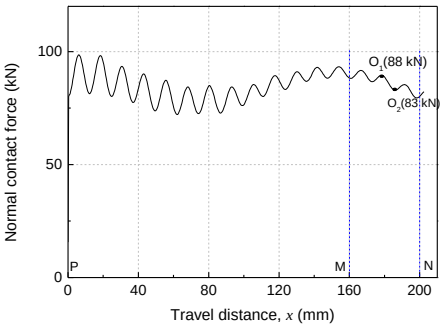

Figure 4. Normal contact forces in scenario A, accounting dynamic effects

As a verification of this property, another point O_2 of 83 kN is picked up, which is at the bottom of a wave. The corresponding p_{max} and p_∞ are 1491 MPa and 1506 MPa respectively. Apparently both O_1 and O_2 produce the same maximum normalized contact pressure of 0.99.

The principle of the above normalization technique can be applied to other cases and scenarios, as well as other quantities such as surface shear stress τ.

3 Influences of lower body width on the contact behavior

The width of the lower body w is varied at $\frac{w}{2b_0} = 1.1, 2, 8$. These three cases are studied for scenarios A (no tractive force) and B (tractive force applies) respectively. In scenario A only the normal contact behavior is investigated, while in scenario B the presence of tractive force enables the study on the shear contact behavior as well.

3.1 Scenario A: no tractive force

In scenario A no driving torque is imposed, thus no tractive force is generated at the contact interface. Three simulations are performed with different lower body widths. The normalized contact pressure distribution along the longitudinal direction is shown in Figure 5. It is worth mentioning that the horizontal axis is normalized by the semi-axis radius of contact area a_∞, which is determined by the Kalker's model for each case. Figure 5 shows that the difference in normalized contact pressure distribution is very small. This suggests the variation of lower body width has little influence on the normal contact behavior, even when the width of contact area is close to the width of lower body.

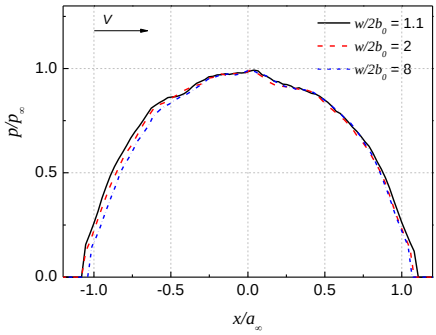

Figure 5. Normalized contact pressure distribution along longitudinal direction in scenario A (no tractive force)

3.2 Scenario B: tractive force applies

In scenario B a driving torque is imposed in such a way that the resulting global tractive force is 25 kN, which is equal to 0.3 times of the total static vertical load 83 kN. Three cases varying lower body width are simulated. Both normal and shear contact behaviors are examined.

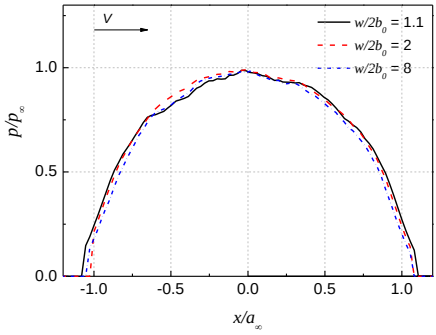

Figure 6. Normalized contact pressure distribution along longitudinal direction in scenario B (tractive force applies)

The normalized contact pressure distribution in scenario B is given in Figure 6. Similarly to scenario A the difference in the normalized pressure distribution is also very small. A cross-scenario comparison is performed by looking at the maximum normalized pressure, as shown in Figure 7. It is observed that the maximum normalized pressures in all three cases and both scenarios are almost the same. Should the value of the maximum normalized pressure be 1.0, it means the calculated maximum pressures from the FE model and the Kalker's model exactly match each other.

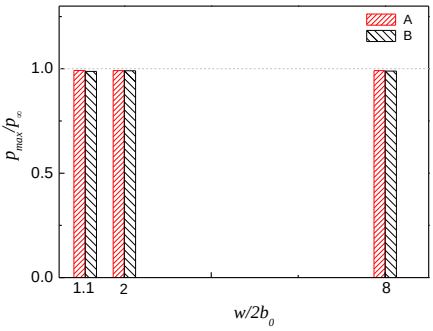

Figure 7. Maximum normalized contact pressure in scenarios A and B

In addition to the normal contact behavior study, the shear contact behavior is also investigated. Figure 8 shows the normalized surface shear stress distribution and the normalized limiting surface shear stress distribution along the longitudinal direction. Similarly to the normal contact solutions the differences in normalized (limiting) shear stresses are almost negligible, although relative larger differences are observed at the border of slip and adhesion regions.

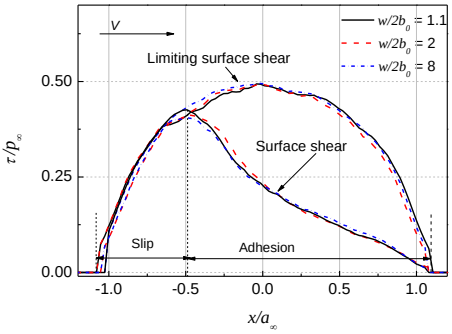

Figure 8. Normalized surface shear stress distribution and normalized limiting surface shear stress distribution along longitudinal direction in scenario B (tractive force applies)

The presence of tractive force can cause micro-slip at the contact interface. When the tractive friction force is smaller than the limiting friction, the partial slip phenomenon occurs. Thus the contact area can be divided into two regions: the slip area and the adhesion area. The normalized slip-adhesion diagram for the case $\frac{w}{2b_0} = 8$ in scenario B is given in Figure 9. Note that both directions are normalized by the longitudinal semi-axis radius of contact area a_∞ from the Kalker's model.

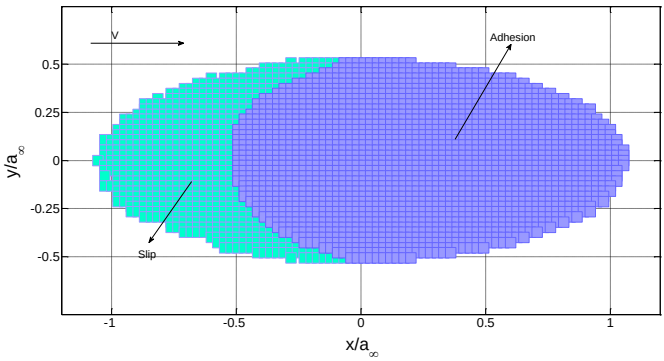

Figure 9. Normalized slip-adhesion area for the case $\frac{w}{2b_0} = 8$ in scenario B (tractive force applies)

The percentage of slip area over the entire contact area reflects the shear behavior of the frictional contact. The diagram of normalized slip area percentage is given in Figure 10. It is observed that the normalized value is affected by the lower body width, but within the limit of 10%. This means the FE model and the Kalker's model may give different values of normalized slip area percentage, but the difference is less than 10%.

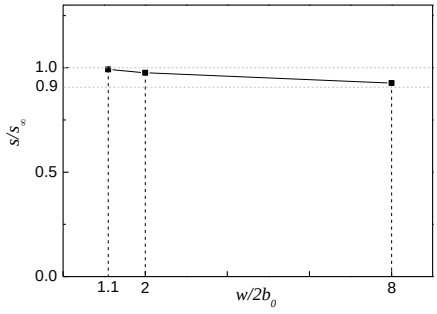

Figure 10. Normalized slip area percentage in scenario B (tractive force applies)

The distributions of the normalized relative velocity of the micro-slip are shown in Figure 11. The curves of the three cases look the same, though small differences are observed at several locations. The differences are examined further by looking at the maximum normalized relative velocity of the micro-slip, as shown in Figure 12. It is found that the difference follows the same trend as in Figure 10. The lower body width has some influences on the maximum normalized relative velocity of the micro-slip, but it is limited within 10%.

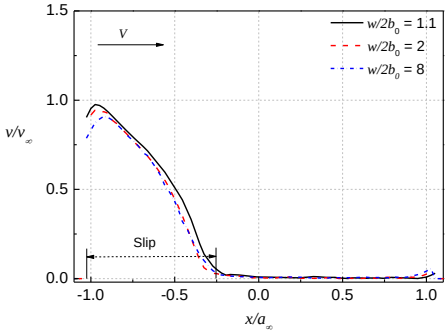

Figure 11. Distributions of the normalized relative velocity of the micro-slip along longitudinal direction in scenario B (tractive force applies)

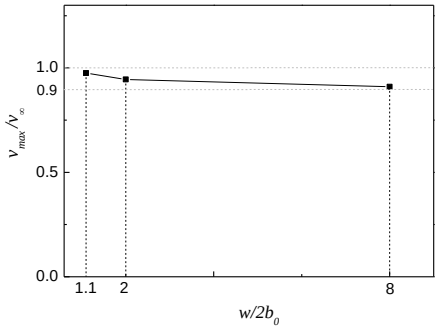

Figure 12. Maximum normalized relative velocity of the micro-slip in scenario B (tractive force applies)

4 Conclusions

In this study the influences of lower body width on the rolling contact of elastic bodies are investigated in detail. Three cases (varying the lower body width) in two scenarios (tractive force applies or not) are compared. It is found that the normal contact pressure distribution, the surface shear stress distribution and the limiting surface shear stress distribution are almost independent of the lower body width. The percentage of slip area over the entire contact area and the relative velocity of the micro-slip are slightly influenced by the lower body width. This finding suggests a possibility to lift the half-space restriction on the Hertz theory and the Kalker's model. It means the Hertz theory and the Kalker's model can still be applied even when the characteristic size of elastic contact bodies is close to the width of the contact area. However it is worth mentioning that the current conclusions are drawn under the condition that the height of lower body is much

larger than the width of contact area. Further study is required to examine whether the influences of lower body height make a difference.

References

[1] N. Anjami, A. Basti, Investigation of rolls size effects on hot ring rolling process by coupled thermo-mechanical 3D-FEA, Journal of Materials Processing Technology, 210 (2010) 1364-1377.

[2] F. Sadeghi, B. Jalalahmadi, T.S. Slack, N. Raje, N.K. Arakere, A Review of Rolling Contact Fatigue, Journal of Tribology, 131 (2009) 041403.

[3] A. Ekberg, E. Kabo, Fatigue of railway wheels and rails under rolling contact and thermal loading—an overview, Wear, 258 (2005) 1288-1300.

[4] H. Hertz, Über die Berührung fester elastischer Körper, Journal für die reine und angewandte Mathematik, 92 (1882) 156-171.

[5] F.W. Carter, On the Action of a Locomotive Driving Wheel, Proceedings of the Royal Society A: Mathematical, Physical and Engineering Sciences, 112 (1926) 151-157.

[6] J.J. Kalker, Three-dimensional elastic bodies in rolling contact, Springer, 1990.

[7] W. Yan, F.D. Fischer, Applicability of the Hertz contact theory to rail-wheel contact problems, Archive of Applied Mechanics, 70 (2000) 255-268.

[8] M. Wiest, E. Kassa, W. Daves, J.C.O. Nielsen, H. Ossberger, Assessment of methods for calculating contact pressure in wheel-rail/switch contact, Wear, 265 (2008) 1439-1445.

[9] X. Zhao, Z. Li, The solution of frictional wheel–rail rolling contact with a 3D transient finite element model: Validation and error analysis, Wear, 271 (2011) 444-452.